ASIAN JOURNAL OF PHARMACEUTICAL SCIENCES 9 (2014) 317–323

HOSTED BY

ELSEVIER

Available online at www.sciencedirect.com

ScienceDirect

journal homepage: http://ees.elsevier.com/ajps/default.asp

Original Research Paper

Development of phosphonate-terminated magnetic mesoporous silica nanoparticles for pH-controlled release of doxorubicin and improved tumor accumulation

*Erxi Che, Long Wan, Ying Zhang, Qinfu Zhao, Xiling Han, Jia Li, Jia Liu, Siling Wang**

Department of Pharmaceutics, Shenyang Pharmaceutical University, Shenyang 110016, China

ARTICLE INFO

Article history:
Received 22 April 2014
Received in revised form
3 July 2014
Accepted 12 July 2014
Available online 27 August 2014

Keywords:
Magnetic mesoporous silica nanoparticles
Doxorubicin
pH-depended release
Tumor accumulation

ABSTRACT

In this study, phosphonate-terminated magnetic mesoporous nanoparticles (pMMSNs) was designed by incorporation of MNPs in the center of mesoporous silica nanoparticles (MSNs) and followed by grafting phosphonate group on to the surface of MMSNs. The carrier exhibited a typical superparamagnetic feature and the saturation magnetization was 4.89 emu/g measured by vibrating sample magnetometer (VSM). pMMSNs had a spherical morphology and a pore size of 2.2 nm. From N_2 adsorption-desorption analysis, pMMSNs had a surface area of 613.4 m^2/g and a pore volume of 0.78 cm^3/g. Phosphonate modification improved the colloidal stability of MMSNs, and the hydrodynamic diameter of pMMSNs was around 175 nm. The hydrophilic phosphonate group significantly enhanced the negative surface charge of MMSNs from −19.3 mV to −28.8 mV pMMSNs with more negative surface charge had a 2.3-fold higher drug loading capacity than that of MMSNs. In addition, the rate and amount of release of doxorubicin (DOX) from DOX/pMMSNs was pH-dependent and increased with the decrease of pH. At pH 7.4, the release amount was quite low and only approximately 17 wt% of DOX was released in 48 h. At pH 5.0 and 3.0, the release rate increased significantly and the release amount achieved 31 wt% and 60 wt% in 48 h, respectively. To evaluate the magnetic targeting performance of pMMSNs, FITC labeled pMMSNs was injected into mice bearing S180 solid tumor. FITC labeled pMMSNs controlled by an external magnetic field showed higher tumor accumulation and lower normal tissue distribution.

* *Corresponding author*. Tel.: +86 24 23986348; fax: +86 24 23986348.
E-mail addresses: silingwang@syphu.edu.cn, silingwang@hotmail.com (S. Wang).
Peer review under responsibility of Shenyang Pharmaceutical University.
http://dx.doi.org/10.1016/j.ajps.2014.07.003

1. Introduction

Magnetic targeting drug delivery systems (MTDDS) based on magnetic nanoparticles and external magnetic field have been considered as a promising approach for localized accumulation of chemotherapeutical agent at the tumor sites [1,2]. Compared with traditional nanotechnology, MTDDS possess the advantages of ease preparation, facile response to external magnetic field and low cost. Moreover, many drug delivery systems depended on the blood circulation can hardly be transported to the tumor sites due to the formation of neovessels, which are often distorted and irregular [3]. Development of MTDDS requires high magnetic susceptibility for optimum magnetic enrichment and loss of magnetization after removal of magnetic field [4]. Concerning the vascular administration of MNPs, good colloidal stability is required. Great efforts have been made to encapsulate MNPs with various shells, such as, polymeric stabilizers and surfactants, e.g., dextran, poly (vinyl alcohol) (PVA), poly (ethylene glycol) (PEG) or oxide surfaces (e.g., SiO_2) to ensure biocompatibility, water dispersibility, as well as appropriated functionalization for further conjugation with bioactive molecules or targeting ligands [5]. In the past decade, mesoporous silica coated MNPs have received much attention due to their advantages: (1) MSNs protect MNPs from being eroded by acidic body fluid; (2) very high surface area and pore volume for drug loading; (3) versatile silanol groups render further modification; (4) good biocompatibility [6,7].

Considering the acidic environment at the tumor sites and more acidic pH of internal cell organelles (pH 4.0–5.0 in the lysosomes and pH 6.0 near the cancer cell membrane) it was wise to design MTDDS possessing pH-stimuli release feature [8,9]. Qu et al. prepared Eudragit-S100 coated MMSNs, which showed high release rate and amount of ibuprofen in simulated proximal intestine fluid, but the polymer was insoluble in simulated gastric fluid resulting in low release accumulation [10]. Yang et al. designed MMSNs coated with a pH sensitive polymer poly methacrylic acid (PMAA). The release rate of doxorubicin from the carrier was faster below its pK_a than that of above its pK_a [11].

The purposes of this study were to incorporate MNPs into the center of MSNs and modify the surface with the hydrophilic phosphonate group (pMMSNs). The phosphonate-termination improved the drug loading capacity of MMSNs by increasing the negative surface charge of MMSNs resulting in a stronger electrostatic interaction between the positively charged DOX and more negatively charged pMMSNs. The DOX release profiles at pH 3.0, 5.0 and 7.4 were significantly different due to the electronic repulsion between DOX and the carriers. FITC labeled pMMSNs were prepared to evaluate the magnetic targeting efficiency of this carrier in vivo under the control of an external magnetic field.

2. Materials and methods

2.1. Materials

Doxorubicin (DOX) in the form of hydrochloride salt was obtained from Haizheng Drug Company (Zhejiang, China). $FeCl_3 \cdot 6H_2O$, $FeSO_4 \cdot 7H_2O$, oleic acid, and Tetraethyl orthosilicate (TEOS) were purchased from Bodi Reagent Company (Tianjin, China). Fluorescein isothiocyanate (FITC) and 3-aminopropyl triethoxysilane (APTES) were purchased from Aladdin (Shanghai, China). Trihydroxyl Silyl Proply Methyl Phosphonate (THPMP) was obtained from Sigma–Aldrich (St. Louis, MO, USA). Other chemicals were of reagent grade and were used without further purification.

2.2. Animals

The male Kunming mice weighing 20–22 g were purchased from the Experimental Animal Center of Shenyang Pharmaceutical University (Shenyang, China). The animal care and experiments were performed in accordance with the guidelines of the local Animal Welfare Committee.

2.3. Preparation of pMMSNs

2.3.1. Preparation of MNPs

Oleic acid stabilized magnetic nanoparticles (MNPs) were prepared via a modified coprecipitation method reported previously [12]. The oleic acid stabilized magnetic nanocrystals were placed in chloroform and the concentration of the magnetic solid was adjusted to 7.5 mg/ml.

2.3.2. Preparation of MMSNs and pMMSNs

pMMSNs were produced by modified sol–gel method [13]. MNPs dispersed in chloroform (1 ml) were added to an aqueous solution of cetyltrimethyl ammonium bromide (CTAB) (20 ml, 12.5 mg/ml) under vigorous ultrasonic to produce a homogeneous oil-in-water microemulsion. Then, chloroform was evaporated by heating at 85 °C to form CTAB stabilized MNPs. And then the system was diluted by distilled water and the pH was adjusted to 12. When temperature was stabilized in 80 °C, 1 ml ethanol was mixed with 1 ml TEOS and then the mixture was added slowly to the aqueous solution containing the CTAB stabilized MNPs. 30 min later, THPMP was added. The solution was stirred for another 3 h followed by collecting the colloidal nanoparticles through centrifugation. CTAB was removed by dispersing the washed sample in 100 ml ethanol solution containing 12 mg/ml ammonium nitrate and heating the mixture at 70 °C for 6 h. The product was then washed with water and ethanol to obtained phosphonate-terminated MMSNs (pMMSNs). MMSNs without phosphonate modification were also prepared but in the absence of THPMP.

2.3.3. Preparation of FITC labeled pMMSNs

1 mg of fluorescein isothiocyanate (FITC) was dissolved in 1 ml absolute ethanol and mixed with 20 μl of 3-aminopropyl triethoxysilane (APTES) for 10 h. 100 mg of pMMSNs was re-dispersed in 100 ml absolute ethanol and heated to 80 °C. After the temperature was stabilized, 0.5 ml of the ethanolic FITC-APTES solution was added slowly to the ethanolic solution containing pMMSNs. The mixture was stirred for 6 h. The synthesized product was re-dispersed in 100 ml of ethanol solution containing 12 mg/ml ammonium nitrate and heating the mixture at 70 °C for 6 h. The product was then washed with water and ethanol to obtain FITC-pMMSNs.

2.4. DOX loading procedure

Positively charged DOX was selected as a model drug. In order to enhance the drug loading capacity, two-steps drug loading process was adopted involving adsorption equilibrium and solvent evaporation. Typically, the adsorption of DOX into mesopores of pMMSNs was carried out by adding pMMSNs to 4 ml of DOX solution (2 mg/ml). The drug/carrier ratio in the loading solution was fasten to 1: 10 (w/w) and then the hybrid was mixed under ultrasonic for 1 h and stirred at room temperature to achieve maximum loading for another 24 h. The process was in a closed container to prevent ethanol evaporation. Finally, the container was opened and ethanol as the solvent was evaporated at 37 °C. The DOX loaded carrier was continually dried at 40 °C under vacuum to remove solvent residue. The drug loaded samples were labeled with DOX/pMMSNs.

2.5. Characterization techniques

The morphology of the samples plated with gold was characterized using TEM (Tecnai G2 20, FEI, USA). Nitrogen adsorption isotherms at −196 °C were measured using a nitrogen adsorption analyzer (V-Sorb 2800P, China). The carriers were degassed to remove physically adsorbed water before analysis. The magnetic curves were analyzed by vibrating magnetometer (Lake Shore 7410, USA) at 300 K. The hysteresis of the magnetization was obtained by changing H between +10,000 Oe and −10,000 Oe. The hydrodynamic diameter, PDI and zeta potential of the samples were measured by photo correlation spectroscopy using a Zetasizer nano (Nano ZS, Malvern Co., UK). TGA-50 instrument (Shimadzu, Japan) was also employed to calculate the weight percentage of phosphonate groups grafted on to the surface MMSNs.

2.6. Analysis of drug content

To determine the drug loading capacity, DOX/MMSNs and DOX/pMMSNs were resuspended in methanol and sonicated for 2 h. The concentration of DOX of the supernatant was determined by ultraviolet (UV) spectroscopy (UV-2000, Unico, USA), while the detection wavelength was 480 nm. The standard curves were linear over the concentration range of 1.0–30 μg/ml. The drug loading capacity (DLC) was calculated by the following equation: $DLC = W_{DOx}/W_{DOx\text{-}carrier}$. Where W_{DOx} is the weight of DOX loaded and $W_{DOx\text{-}carrier}$ is the weight of DOX loaded carrier.

2.7. In vitro DOX release study

A typical in vitro drug release experiment was performed as follows. An aliquot of 20 mg of drug/carrier composite was immersed in 20 ml of 0.1 M phosphate buffer solution of required pH (pH 3.0, pH 5.0 and pH 7.4). The release medium was stirred at 100 rpm and at 37 °C. At predetermined sampling time, 4 ml of medium was extracted for measurement, and then put back to the container. The amount of DOX in the medium was determined by UV-spectroscopy at a detection wavelength of 480 nm for all pH values. The experiments were performed in triplicate.

2.8. Ex vivo tissue imaging

The in vivo imaging system (FX Pro, Kodak, USA) was applied to evaluate the magnetic targeting efficiency of pMMSNs controlled by an external magnet field in Kunming mice bearing S180 tumor. Briefly, when tumor sizes reached 1500 mm^3, mice were received the FITC labeled pMMSNs (10 mg/ml) intravenously and the blank group receive saline. The test group was then treated with permanent magnet attached to the surface of the tumor of the mice for 1 h. Mice were scarified at 2 h, and then tumor and normal tissues were imaged with appropriate wavelength (λ_{ex}: 480 nm, λ_{em}: 535 nm).

3. Results and discussion

3.1. Preparation of MNPs, MMSNs and pMMSNs

In this study, MNPs were synthesized according to the traditional coprecipitation method and stabilized with oleic acid [13]. A simple sol–gel method was applied to prepare monodispersed MNPs embedded in mesoporous silica shell. Scheme 1 shows a typical synthetic process of pMMSNs in. As previously reported, pre-existing CTAB stabilized MNPs served as the nucleation seeds [13,14]. Under basic conditions, the silica oligomers which were generated by the hydrolysis of TEOS, self-assembled with surfactant micelles to form CTAB/silica mesostructured nano-composites, which subsequently deposited on the magnetic seeds to construct the shell framework. However, in the case of MSNs, the mesostructured nano-composites aggregated together directly and grew to the whole particle by further condensation of silica species. CTAB served not only as the organic template for the formation of mesopores but also as the secondary surfactant to transfer MNPs from organic solvent to aqueous phase [15]. The surface of MMSNs was modified with hydrophilic phosphonate groups shortly after the particle formation resulted in increased stability and dispersibility of the carrier in aqueous solution even after drying process. Previous research had reported that MMSNs easily aggregated and settled to the bottom quickly after drying and re-dispersing process. The irreversible aggregation might be attributed to the interparticle hydrogen-bonding interaction between the surface silanol groups and can be prevented by grafting hydrophilic molecules on to the surfaces [16,17].

3.2. Characterization of MNPs, MMSNs and pMMSNs

Fig. 1A presents the TEM images of oleic acid modified MNPs with a diameter of around 10 nm. However, the nanoparticles showed a slight aggregation. MNPs with a diameter of about 10 nm behaved superparamagnetism which meant that they were magnetic only under the controlled of external magnetic field and became inactive once the external magnetic field is removed. Fig. 1B shows that pMMSNs were discrete spheres with a diameter of around 100 nm. The appearance of the pores was distorted and ran radically to the surface. MNPs were individually imbedded in the center of silica shell due to vigorous ultrasonic stirring in the stage of transforming MNPs

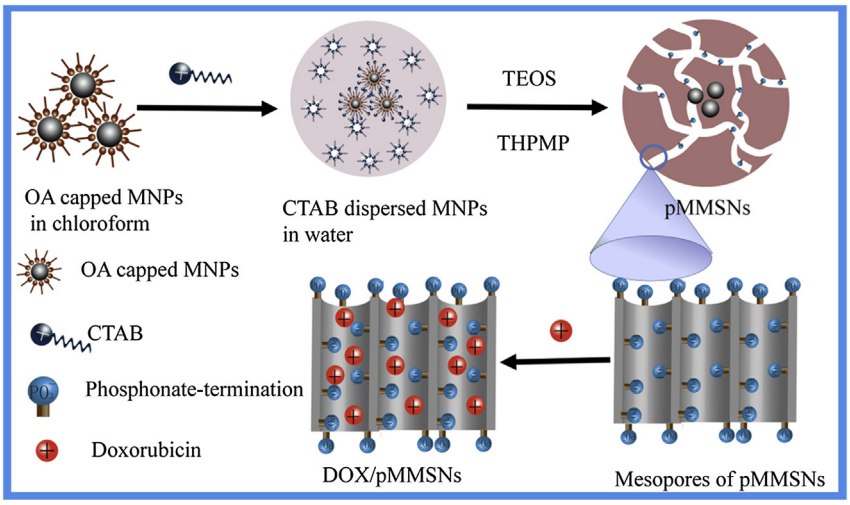

Scheme 1 – Schematic preparation process of MMSNs, pMMSNs, DOX loaded pMMSNs.

from organic solvent to aqueous solvent. The pore space supplied to further DOX laden.

The pore structure of MMSNs and pMMSNs were measured through N_2 adsorption-desorption analysis. Fig. 2A shows the N_2 adsorption isotherms of MMSNs and pMMSNs, which were typical type IV isotherms with two steps confirming their mesoporous structure according to the IUPAC classification. Compared with MMSNs, the adsorbed nitrogen amount of pMMSNs was slightly reduced, but the shape of the hysteresis remained unchanged. The BET surface area, pore volume and pore diameter of MMSNs were 923.6 m^2/g, 1.48 cm^3/g and 2.8 nm, respectively. The parameters of pMMSNs were reduced to 613.4 m^2/g, 0.78 cm^3/g, and 2.2 nm, respectively (Table 1). These results suggested that phosphonate-termination did not destruct the pore structure. However, phosphonate-group distributed on the interior pore walls and exterior surface of MMSNs occupied some pore space which could be used to storage drugs molecules.

Fig. 3 illustrates the field-dependent magnetization curves of MNPs, MMSNs and pMMSNs measured at 300 K. They exhibited a typical superparamagnetism and no hysteresis was observed in low fields. The saturated magnetization value of MNPs was 37.5 emu/g. But it dramatically decreased to 6.74 emu/g and 4.89 emu/g for MMSNs and pMMSNs. As shown in Fig. 3 (inserted), pMMSNs with superparamagnetic characteristic and high magnetization value could quickly respond to external magnetic field and redisperse in aqueous solution once the external magnetic field was removed and with gentle shaking or sonication.

Fig. 4 shows the thermogravimetric analysis (TGA) of MMSNs and pMMSNs. The decline in the curves started from a low temperature of about 50 °C. This might be attributed to the evaporation of absorbed water tightly bound to the carriers. TGA curves demonstrated that the weight loss of MMSNs was 6 wt%, while that of pMMSNs was 14.9 wt%. Thus, the content of phosphonate-termination was about 8.9 wt %.

The particle sizes and zeta potential measurements of MMSNs and pMMSNs were performed using dynamic light scatter (DLS) technique to evaluate the dispersibility, stability and surface charge potential after each preparation steps (Table 2). Bare MMSNs had a negative surface charge of around −20 mV in PBS solution at pH 7.4, mean hydrodynamic diameter of 166.4 nm and a narrow PDI of 0.201. The particle size measured by DLS was higher than the particle size observed from TEM image of that sample. This could be attributed to the formation of hydrodynamic shell of MMSNs and slight aggregates between nanoparticles. The hydrodynamic diameter and PDI of pMMSNs were 175 nm and 0.218,

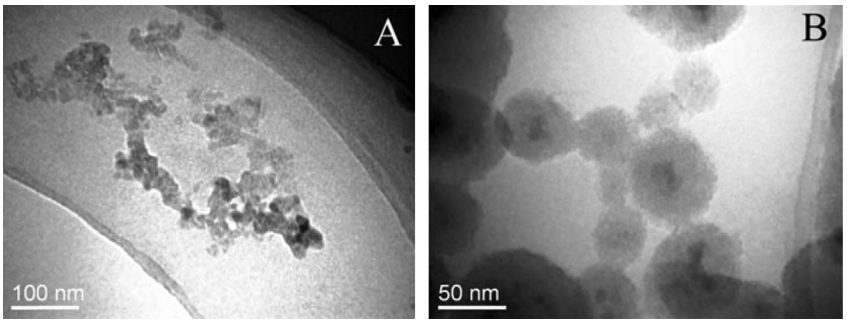

Fig. 1 – TEM images of (A) MNPs and (B) pMMSNs.

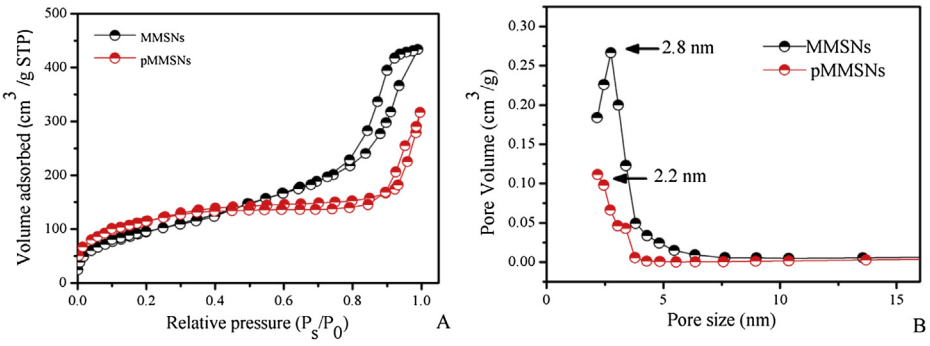

Fig. 2 – (A) N_2 adsorption-desorption isotherms and (B) pore size distributions of MMSNs and pMMSNs.

respectively. Once, the material was dried and re-dispersed in aqueous solution, MMSNs without phosphonate modification easily aggregated and settled down to the bottom. On the other hand, pMMSNs were stable when re-dispersed in aqueous solution, and their hydrodynamic size and PDI showed a slight increasement. Moreover, pMMSNs leaded to more negative surface charge value of −28.8 mV in PBS solution at pH 7.4. This could be explained that the phosphonate groups have a higher pK_a value than that of the silanol groups.

3.3. *Drug loading capacity (DLC) and in vitro release study*

In this study, positively charged DOX was selected as a model drug to investigate the drug loading capacity (DLC) of the carriers and to study the pH-dependent release of DOX/pMMSNs. Table 1 shows that the DLC of pMMSNs (6.9 wt%) was higher than that of MMSNs (2.8 wt%). The probable reasons for the enhanced DLC of DOX in pMMSNs were as follows. The electronic attraction between negatively charged carriers and positively surface charge of DOX might be the main factor that affected DLC. Even though, pMMSNs had lower surface area and pore volume than that of MMSNs, the DLC value of DOX/pMMSNs was 2.3-fold higher than that of DOX/MMSNs. Therefore, we could speculate that the surface area and pore volume of pMMSNs were high enough for DOX incorporation.

Drug delivery systems with the pH-responsive release profile mean that drugs do not or hardly release in normal tissues and blood (pH ~ 7.4), but can responsively release in tumor tissues, or even within cancer cells, to selectively kill cancer cells (pH 3.0–5.0) [18]. The release profiles of DOX from DOX/MMSNs and DOX/pMMSNs were investigated in PBS solution at three different pH. The pH 3.0 and pH 5.0 represented the acidic environment of tumor tissues, while pH 7.4 represented the neutral pH of normal tissues and blood. On the whole, the observed release rate and amount of DOX from DOX/MMNSs and DOX/pMMSNs increased with the decrease in the pH values. Fig. 5A shows that, at pH 3.0, the release rate of DOX from DOX/MMSNs was relatively fast and 63% amount of DOX diffused to release medium at 48 h. At pH 5.0, the release rate and amount of DOX from DOX/MMSNs were decreased reached 51% at 48 h. However, at pH 7.4, the release curve of DOX from DOX from DOX/MMSNs was almost flat and the release accumulation was 14%. The reasons for this phenomenon was that amine groups from doxorubicin are partially deprotonated at pH 7.4 (pK_a = 8.22), while they are fully protonated at pH 3.0 and 5.0. On the other hand, MMSNs have a higher total positive charge at pH 5.0 and even higher positive charge at pH 3.0 because of the presence of surface silanol groups (pK_a = 6.8) [19]. Therefore, the electronic repulsion between DOX and the carrier contributed to the pH-dependent release profile of DOX/MMSNs.

Table 1 – Characteristics of MMSNs and pMMSNs.

Sample	S^a_{BET} (m^2/g)	V^b_t (cm^3/g)	D^c_{BJH} (nm)	Drug loading capacity (wt%)	Saturation magnetization (emu/g)
MMSNs	923.6	1.48	2.8	2.8	6.74
pMMSNs	613.4	0.78	2.2	6.9	4.89

S^a_{BET} is the BET surface area calculated using experimental points at a relative pressure of P/P_0. V^b_t is the total pore volume determined at a relative pressure of 0.9814. D^c_{BJH} is the pore diameter calculated by the BJH method on the branches of the nitrogen desorption isotherms.

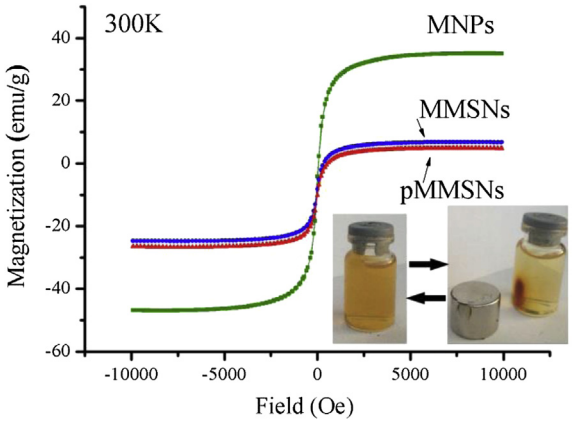

Fig. 3 – Field-dependent magnetization of MNPs, MMSNs and pMMSNs and photograph demonstrating high magnetic responsiveness of pMMSNs with an external magnetic field (inserted).

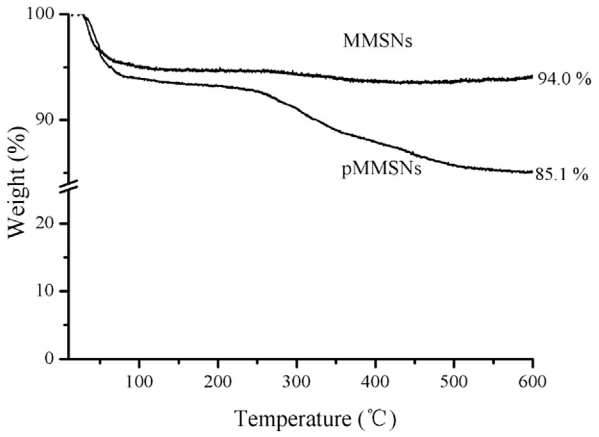

Fig. 4 – TGA curves of MMSNs and pMMSNs at 300 K.

Table 2 – Hydrodynamic size, size distribution and zeta potential values of MMSNs and pMMSNs.

Sample	Hydrodynamic size (nm)	PDI	Zeta potential (mV)
MMSNs	166.4 ± 14.3	0.201 ± 0.012	−19.3
pMMSNs	175.7 ± 11.4	0.218 ± 0.0089	−28.8
pMMSNs (drying and re-dispersing)	232.5 ± 10.9	0.267 ± 0.023	–

Fig. 5B presents sustained release patterns of DOX from the phosphonate modified MMSNs (pMMSNs) in PBS solution at three different pH. At pH 3.0, the release pattern showed a burst release amount of 31% at the initial 4 h and then the release rate turned slow to reach a total release accumulation of 60%. At pH 5.0, the release rate and amount of DOX from DOX/pMMSNs decreased and only 43% of DOX dissolved in the medium. At pH 7.4, the whole release amount of DOX from DOX/pMMSNs was also incomplete with a final accumulation of 17% at 48 h. The reasons for the sustained release behavior of DOX from phosphonate modified carrier may be that phosphonate modification made the surface charge potential of MMSNs even more negative, thus the attractive interaction between DOX and pMMSNs was stronger than the attractive force between DOX and MMSNs.

3.4. *In vivo distribution of pMMSNs (MF^+) and pMMSNs (MF^-)*

To demonstrate that pMMSNs could be controlled by external applied magnetic field, FITC labeled pMMSNs was injected intravenously into mice bearing S180 tumor. The test group then was fixed with an external magnetic field at the solid tumor for 1 h, referred to as pMMSNs (MF^+). The contrast group also received the same formulation but without an applied magnetic field (MF^-). Also, mice received saline was treated as controlled group. Since the FITC fluorescence signal had poor penetration ability in deep tissues and the background fluorescence intensity of mice was high, mice were sacrificed at 2 h after administration and ex vivo fluorescence intensity images of the major organs and tumors were obtained, as shown in Fig. 6. The fluorescence intensities in the heart and spleen of mice of the two groups were very low. Enhanced fluorescence intensity was observed in the tumor of mice treated with pMMSNs (MF^+). On the other hand, the fluorescence intensity in liver and lung of mice treated with pMMSNs (MF^-) was obviously higher than that of mice treated with pMMSNs (MF^+). This phenomenon was attributed to that without external magnetic field, the discontinuous gaps in the endothelium which lines the sinusoidal walls of liver allow the passive entrapment of pMMSNs [20,21]. Moreover, macrophages in liver had great association with the nanoparticles than other types of cells [22]. The high lung affinity of pMMSNs was due to hydrodynamic size increased in serum which leaded to transient association with capillary in lung. A high tumor accumulation of pMMSNs (MF^+) demonstrated the feasibility of our designed magnetic targeting drug delivery system.

4. Conclusion

The results of this paper showed that phosphonate-terminated magnetic mesoporous silica nanoparticles (pMMSNs) with a saturation magnetization of 4.89 emu/g and a hydrodynamic diameter of around 175 nm were prepared. The negative surface charge (−28.8 mV) and surface area of 613.4 m^2/g warranted successful loading of DOX using a two-steps

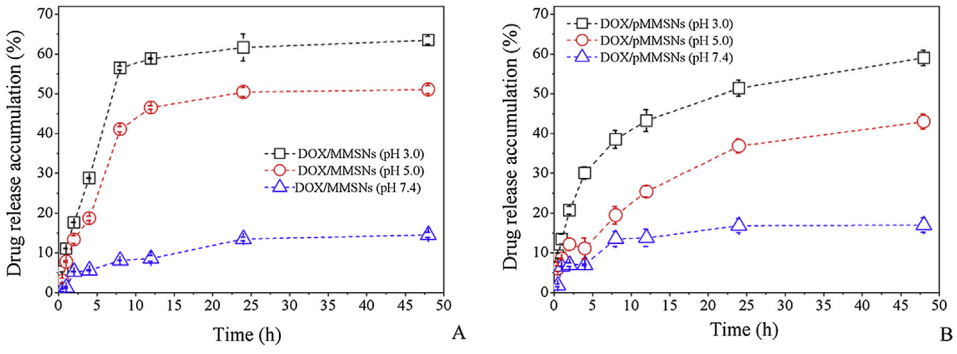

Fig. 5 – In vitro release profiles of DOX from (A) DOX/MMSNs and (B) DOX/pMMSNs in PBS solution at pH 3.0, 5.0 and 7.4.

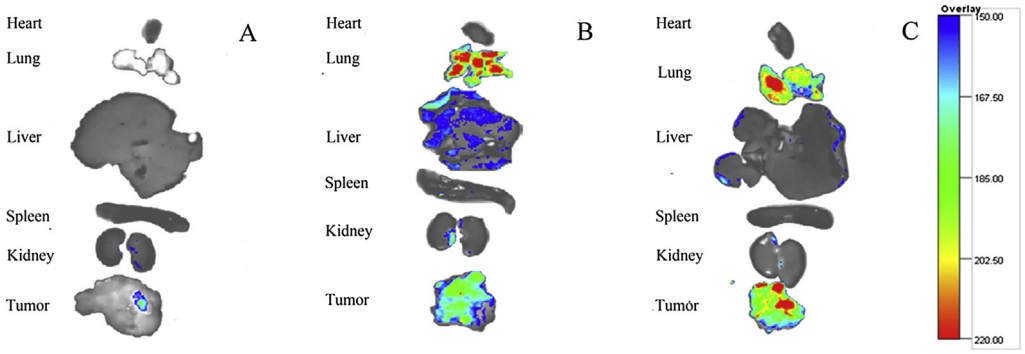

Fig. 6 – Ex vivo optical images of tumors and other organs of S180 tumor bearing mice sacrificed at 2 h after intravenous injection of FITC labeled pMMSNs. (A) S180 tumor bearing mice treated with saline; (B) S180 tumor bearing mice treated with pMMSNs (MF^-); (C) S180 tumor bearing mice treated with pMMSNs (MF^+).

method including adsorption equilibrium and solvent evaporation. The in vitro release profiles of DOX/pMMSNs were pH-depended. At lower pH (3.0 and 5.0), DOX release rate and release amount of DOX was higher compared to that of at pH 7.4 and this can be attributed to the decreased electrostatic interaction between the negative surface charge of pMMSNs and the entrapped DOX from the nanoparticles. Moreover, ex vivo tissue fluorescence intensity measurement showed that under the facilitation of external magnetic field, the distribution of pMMSNs (MF^+) was improved via a higher tumor retention and lower distribution in normal tissues than that of pMMSNs (MF^-). We believe that these results may open the possibilities for combining magnetic targeting drug delivery system and pH-responsive release of doxorubicin to cancerous tissue.

REFERENCES

[1] Cole A, Yang V, David A. Cancer theranostics: the rise of targeted magnetic nanoparticles. Trends Biotechnol 2011;29:323–332.
[2] Arruebo M, Fernández-Pacheco R, Ibarra M, et al. Magnetic nanoparticles for drug delivery. Nano Today 2007;2:22–32.
[3] Mody V, Cox A, Shah S, et al. Magnetic nanoparticle drug delivery systems for targeting tumor. Appl Nanosci 2014;4:385–392.
[4] Reddy L, Arias J, Nicolas J, et al. Magnetic nanoparticles: design and characterization, toxicity and biocompatibility, pharmaceutical and biomedical applications. Chem Rev 2012;112:5818–5878.
[5] Butterworth M, Illum L, Davis S. Preparation of ultrafine silica-and PEG-coated magnetite particles. Colloid Surf A 2001;179:93–102.
[6] Lee J, Lee N, Kim T, et al. Multifunctional mesoporous silica nanocomposite nanoparticles for theranostic applications. Acc Chem Res 2011;44:893–902.
[7] Li Z, Barnes J, Bosoy A, et al. Mesoporous silica nanoparticles in biomedical applications. Chem Soc Rev 2012;41:2590–2605.
[8] Pillay C, Elliott E, Dennison C. Endolysosomal proteolysis and its regulation. Biochem J 2002;363:417–429.
[9] Griffiths J. Are cancer cells acidic? Br J Cancer 1991;64:425–427.
[10] Xing R, Lin H, Jiang P, et al. Biofunctional mesoporous silica nanoparticles for magnetically oriented target and pH-responsive controlled release of ibuprofen. Colloid Surf A 2012;403:7–14.
[11] Wen H, Guo J, Chang B, et al. pH-responsive composite microspheres based on magnetic mesoporous silica nanoparticle for drug delivery. Eur J Pharm Biopharm 2013;84:91–98.
[12] Liu C, Guo J, Yang W, et al. Magnetic mesoporous silica microspheres with thermo-sensitive polymer shell for controlled drug release. J Mater Chem 2009;19:4764–4770.
[13] Kim J, Lee JE, Lee J, et al. Magnetic fluorescent delivery vehicle using uniform mesoporous silica spheres embedded with monodisperse magnetic and semiconductor nanocrystals. J Am Chem Soc 2006;128:688–689.
[14] Nooney R, Thirunavukkarasu D, Chen Y, et al. Self-assembly of mesoporous nanoscale silica/gold composites. Langmuir 2003;19:7628–7637.
[15] Fan H, Yang K, Boye DM, et al. Self-assembly of ordered, robust, three-dimensional gold nanocrystal/silica arrays. Science 2004;304:567–571.
[16] Xu H, Yan F, Monson E, et al. Room-temperature preparation and characterization of poly (ethylene glycol)-coated silica nanoparticles for biomedical applications. J Biomed Mater Res A 2003;66:870–879.
[17] Bagwe R, Hilliard L, Tan W. Surface modification of silica nanoparticles to reduce aggregation and nonspecific binding. Langmuir 2006;22:4357–4362.
[18] Gao W, Chan J, Farokhzad O. pH-responsive nanoparticles for drug delivery. Mol Pharm 2010;7:1913–1920.
[19] Knežević N, Trewyn B, Lin V. Light-and pH-responsive release of doxorubicin from a mesoporous Silica-Based nanocarrier. Chem Eur J 2011;17:3338–3342.
[20] Gratton S, Pohlhaus P, Lee J, et al. Nanofabricated particles for engineered drug therapies: a preliminary biodistribution study of PRINT™ nanoparticles. J Control Release 2007;121:10–18.
[21] Xie G, Sun J, Zhong G, et al. Biodistribution and toxicity of intravenously administered silica nanoparticles in mice. Arch Toxicol 2010;84:183–190.
[22] Yu T, Malugin A, Ghandehari H. Impact of silica nanoparticle design on cellular toxicity and hemolytic activity. Acs Nano 2011;5:5717–5728.